Metal–Organic Framework Nanoparticles Induce Pyroptosis in Cells Controlled by the Extracellular pH

ADVANCED MATERIALS
www.advmat.de

Metal–Organic Framework Nanoparticles Induce Pyroptosis in Cells Controlled by the Extracellular pH

Evelyn Ploetz, Andreas Zimpel, Valentina Cauda, David Bauer, Don C. Lamb, Christoph Haisch, Stefan Zahler, Angelika M. Vollmar, Stefan Wuttke, and Hanna Engelke**

Ion homeostasis is essential for cellular survival, and elevated concentrations of specific ions are used to start distinct forms of programmed cell death. However, investigating the influence of certain ions on cells in a controlled way has been hampered due to the tight regulation of ion import by cells. Here, it is shown that lipid-coated iron-based metal–organic framework nanoparticles are able to deliver and release high amounts of iron ions into cells. While high concentrations of iron often trigger ferroptosis, here, the released iron induces pyroptosis, a form of cell death involving the immune system. The iron release occurs only in slightly acidic extracellular environments restricting cell death to cells in acidic microenvironments and allowing for external control. The release mechanism is based on endocytosis facilitated by the lipid-coating followed by degradation of the nanoparticle in the lysosome via cysteine-mediated reduction, which is enhanced in slightly acidic extracellular environment. Thus, a new functionality of hybrid nanoparticles is demonstrated, which uses their nanoarchitecture to facilitate controlled ion delivery into cells. Based on the selectivity for acidic microenvironments, the described nanoparticles may also be used for immunotherapy: the nanoparticles may directly affect the primary tumor and the induced pyroptosis activates the immune system.

Ions are important signals for cells, and maintenance of their intracellular concentration is essential for survival. They activate signaling cascades and regulate enzyme activity and osmotic pressure as well as redox potential and pH.[1] Sudden overdoses of ions in the cytosol or other intracellular compartments often induce programmed cell death. High amounts of cytosolic calcium, for example, induce apoptosis,[2] and ferroptosis is triggered by an overdose of lysosomal iron.[3] Controlled introduction of ions into certain cellular compartments would allow for an understanding of how ions influence cellular processes in these compartments. At the same time, it bears high therapeutic potential, specifically the induction of programmed cell death. However, due to the profound importance of ion concentrations, cells maintain their ion balance very carefully. Complex procedures ensure uptake, storage, and release of the necessary amounts of ions and strictly prevent external manipulation of ion levels.[1a,4] To overcome these regulatory mechanisms, small molecules, such as ionophores or inhibitors of cellular ion channels, have been used previously.[5] While they allow for manipulation of ion homeostasis to a certain extent, they often also interact with off-target molecules obstructing the investigation of the influence

Dr. E. Ploetz, Dr. A. Zimpel, Prof. D. C. Lamb, Dr. H. Engelke
Department of Chemistry and Center for NanoScience (CeNS)
LMU Munich
Munich 81377, Germany
E-mail: hanna.engelke@cup.uni-muenchen.de
Dr. E. Ploetz, Prof. D. C. Lamb
Nanosystems Initiative Munich (NIM)
LMU Munich
Munich 81377, Germany
Dr. E. Ploetz, Prof. D. C. Lamb
Center for Integrated Protein Science Munich (CiPSM)
LMU Munich
Munich 81377, Germany

The ORCID identification number(s) for the author(s) of this article can be found under https://doi.org/10.1002/adma.201907267.

DOI: 10.1002/adma.201907267

Prof. V. Cauda
Department of Applied Science and Technology
Politecnico di Torino
Torino 10129, Italy
D. Bauer, Prof. C. Haisch
Department of Chemistry
TU Munich
Munich 81377, Germany
Prof. S. Zahler, Prof. A. M. Vollmar
Department of Pharmacy
LMU Munich
Munich 81377, Germany
Prof. S. Wuttke
BCMaterials, Basque Center for Materials
UPV/EHU Science Park
Leioa 48940, Spain
E-mail: stefan.wuttke@bcmaterials.net
Prof. S. Wuttke
Ikerbasque
Basque Foundation for Science
Bilbao 48013, Spain

of ions. Moreover, their molecular structure makes it difficult to dissect the effect of the ion concentration from other reactive groups in the molecule. Direct, controlled intracellular introduction of ions would enable a study of the mechanisms of ion-triggered cellular processes on an atomistic level eliminating any obstructing effects of mediator molecules.

Hybrid metal–organic framework (MOF) nanoparticles offer an option to overcome the challenge of direct and controlled ion delivery.[6] They consist of high amounts of ions coordinated to organic linker molecules and the specific ion and organic linker can be chosen from a plethora of building blocks to match the requirements of the application.[7] Thus, they can be built from the ions that are to be released in the cells. The nanoscale size of MOF nanoparticles facilitates cellular internalization. To prevent cellular recognition of the ions on the surface of MOF nanoparticles and to overcome subsequent cellular regulation mechanisms, the nanoparticle surface can be functionalized, for example, with polymers[6c,8] or lipid coatings.[9] Finally, their structure and chemical stability can, in principle, be designed to meet the desired degradation conditions and kinetics, which would control the location and kinetics of ion release. An example would be degradation under the reductive milieu of the lysosome or by chelation agents.[9b] Pore size with respect to, for example, the chelating molecule will then control the reaction kinetics. A large pore size combined with a relatively small degrading molecule that can access all interaction sites will, in most cases, enable sudden release. Hence, the specific hybrid nanoarchitecture of MOF nanoparticles combined with their tailorable surface functionalization renders them a promising candidate for stealth ion transport into cells followed by sudden release of high amounts of ions under controlled conditions.

In this study, we show that lipid-coated MIL-100(Fe) MOF nanoparticles,[10] consisting of iron (Fe^{3+}) and trimesic acid, are able to introduce high amounts of iron ions into cells. The lipid coating facilitates cellular uptake via endocytosis. Acidification of the extracellular pH subsequently leads to intracellular degradation of MOF nanoparticles and release of iron followed by cell death and lysis. When studying this process in detail, we found that degradation of MOF nanoparticles triggers pyroptosis, an inflammatory form of programmed cell death.[11] Its dependence on the extracellular pH provides an external trigger for pyroptosis induction. This shows how delivery of ion overdoses can lead to unforeseen effects, such as the activation of pyroptosis in this particular case. Similar effects may be found when the principle of ion delivery via controlled degradation of lipid-coated MOF nanoparticles is applied to other ions.

MIL-100(Fe) nanoparticles were synthesized as reported in literature (for characterization and detailed synthesis, see Supporting Information).[12] To facilitate their cellular uptake via endocytosis, the nanoparticles were coated with 1,2-dioleoyl-*sn*-glycero-3-phosphocholine (DOPC) (see **Figure 1**a; Figure S1, Supporting Information). Coating was performed by mixing the MIL-100(Fe) nanoparticles with DOPC-liposomes and employing lipid fusion as previously described.[9b,13] Successful coating was confirmed with nitrogen-sorption measurements and infrared spectroscopy (Figure 1b; Figure S2, Supporting Information). The resulting DOPC-coated MIL-100(Fe) nanoparticles (denoted here as Lip-MOF) had a hydrodynamic radius of 250 nm as determined by dynamic light scattering (Figure 1c). Electron microscopy and X-ray diffraction indicated that the properties of MOF nanoparticles are conserved upon the lipid coating (Figure 1d,e; Figures S3 and S4, Supporting Information).

Next, we investigated the effect of Lip-MOFs on cells. We loaded them with the dye calcein prior to liposome coating such that the fluorophore is quenched by the MOFs and only becomes visible upon the degradation of the MOFs. The calcein-loaded Lip-MOFs were brought in contact with HeLa cells (**Figure 2**a; see also Movie S1, Supporting Information). Directly after incubation, the particles are not visible since the calcein is still quenched within the nanoparticles. About 40 h after incubation, calcein was visible, indicating that the Lip-MOF have degraded. Shortly afterwards, we observed a sudden spread of the calcein dye all over the cell followed by a burst and deflation of the entire cell. An MTT test 72 h after incubation confirmed the observed toxicity of the Lip-MOF with an IC_{50} of ≈3 μg mL^{-1} (Figure 2b, green squares). Strikingly, this toxicity was strongly dependent on the extracellular pH: the extracellular pH of the medium covering metabolizing HeLa cells decreases over time.[14] The described cell death was observed in experiments without exchange of the medium resulting in a decreased pH value. When the pH was kept constant at pH 7.4 by daily exchange of the medium, cell viability was not affected significantly (Figure 2b, orange circles). The toxicity of Lip-MOF could be restored by daily changes of medium at pH 7.2 (Figure 2b, red triangles). To test whether this effect was really due to iron delivery and not based on trimesic acid, we added Tiron to the medium (Figure 2b, blue triangles). Tiron chelates Fe^{3+} as present in Lip-MOF and will transport the ions across the cellular membranes reducing the local, intracellular iron concentration. Addition of Tiron inhibits the effect of Lip-MOF confirming the high amount of delivered iron as the cause of the observed cell burst. Iron oxide nanoparticles, however, did not induce this effect (see Figure S5, Supporting Information), nor did MIL-88A nanoparticles consisting of Fe^{3+} and fumaric acid.[9b,13b] Hence, cell lysis is due to intracellular iron delivery of Lip-MOF controlled by the extracellular pH. This is an entirely new effect of MOF nanoparticles.

To gain a better understanding of this unusual lytic effect, we first studied the cellular internalization mechanism. Cellular uptake of Lip-MOF was quantified 30 min after incubation via inductively coupled plasma optical emission spectrometry (ICP-OES) (Figure 2c). Comparison between the uptake at 37 and 4 °C shows a significant reduction in nanoparticle uptake at reduced temperatures. This suggests that energy-dependent endocytosis may be the main uptake pathway for Lip-MOF as reported for MOF nanoparticles in literature.[15] Uncoated MIL-100(Fe) on the contrary did not show any toxicity to cells (Figure S6, Supporting Information) and its uptake was not significantly reduced at 4 °C, that is, endocytosis was not the main uptake pathway. This suggests that the lipid bilayer mediates efficient uptake via endocytosis as the first important step for the pH-dependent toxicity of Lip-MOFs. Further investigation on the uptake mechanism was performed by inhibition of different endocytosis pathways with Dynasore, Cytochalasin D, and Filipin, respectively. The results suggest clathrin-mediated endocytosis to be the main uptake pathway as Dynasore showed the strongest reduction in iron uptake measured by ICP-OES (Figure S7, Supporting Information). This is

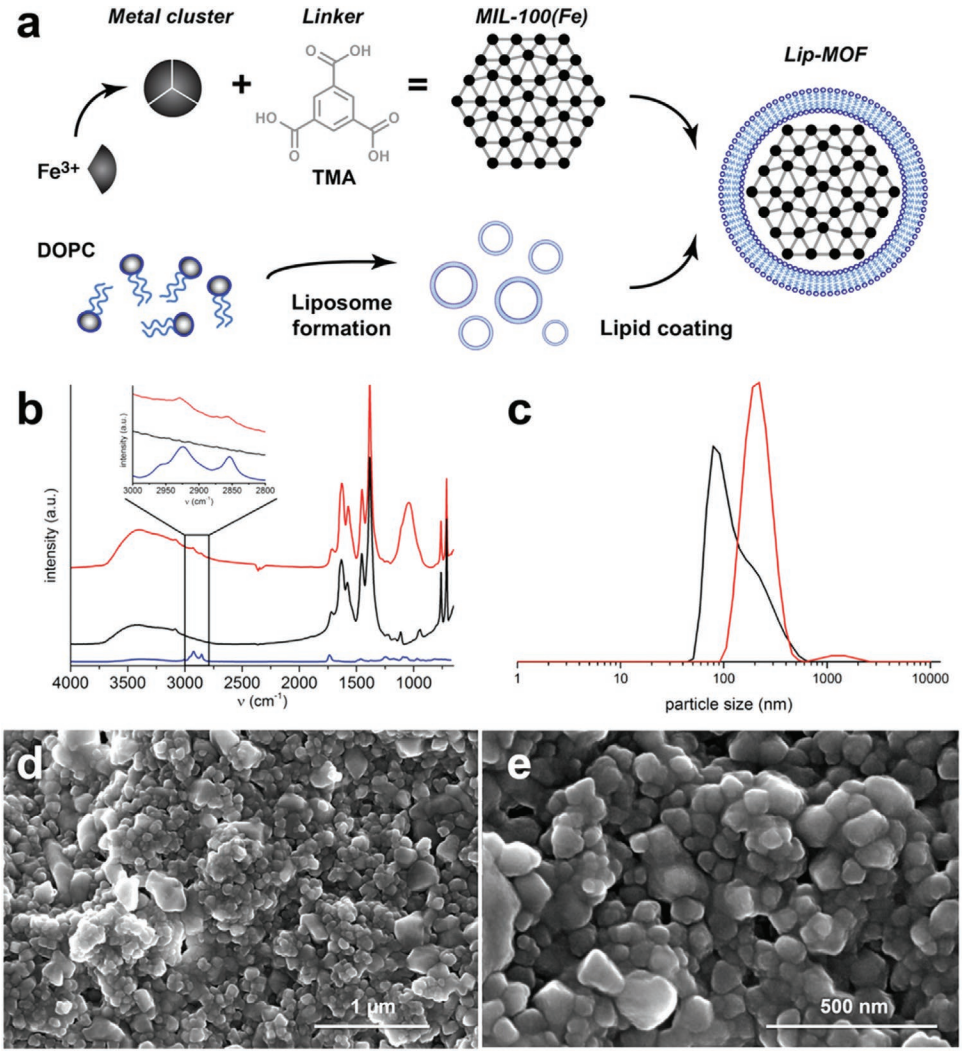

Figure 1. Synthesis and characterization of Lip-MOF nanoparticles. a) Synthesis route. b) IR spectroscopy reveals successful lipid coating. IR spectra of Lip-MOF nanoparticles (red), unfunctionalized MIL-100(Fe) nanoparticles (black), and pure DOPC (blue). The inset shows a magnification of the significant aliphatic C–H stretching vibrations present in DOPC and Lip-MOF. c) Size determination of Lip-MOFs via dynamic light scattering of unfunctionalized MIL-100(Fe) nanoparticles (black) and Lip-MOF (red) in DPBS. Lip-MOF show a slight increase in average size compared to uncoated MOFs and possess a homogeneous size distribution around 250 nm. d,e) SEM images of uncoated (d) and lipid-coated MIL-100(Fe) (e) nanoparticles at 150 000× magnification.

in accordance with literature.[15] Lysosomal markers colocalized with the distinct spots of the dye that were observed about 40 h after cell incubation with Lip-MOFs (Figure 2d; Figure S8, Supporting Information). Thus, 40 h after incubation, the Lip-MOF were internalized via endocytosis and reached the acidic lysosome. In the lysosome, the nanoparticles are degraded and the dye is no longer quenched. This leads to the observed fluorescence of the dye after 40 h. Some of the dye is still contained within the lysosomes and visible as puncta. Shortly afterwards, the fluorescence spreads throughout the cell, indicating degradation of the lysosomes. Lysosomal degradation of the Lip-MOF was also confirmed by immediate decomposition in artificial lysosomal fluid (ALF), which simulates the lysosomal environment. Quantitative UV–vis measurements of an iron marker revealed within errors a complete decomposition of the Lip-MOF after only 1 h in ALF (Figure S9, Supporting Information). In simulated body fluid, which simulates the environment in the blood rather than within lysosomes, no decomposition of the Lip-MOF could be detected (Figure S9, Supporting Information). This decomposition of the Lip-MOF in the lysosome is a crucial part of its toxicity. Accordingly, whenever a burst of cells was observed, it was preceded by calcein fluorescence in the lysosome as a reporter of Lip-MOF. At constant extracellular pH 7.4, when cell death is not induced, this calcein fluorescence in the lysosome was not detected (Figure S10, Supporting Information).

ALF contains citric acid, which causes degradation of the Lip-MOF into its building blocks, that is, iron ions and trimesic acid. The role of citric acid in the ALF is to simulate lysosomal enzyme activity. In order to find the origin of the lysosomal degradation of Lip-MOF, we investigated the influence of lysosomal enzymes. A direct degradation of the Lip-MOF by

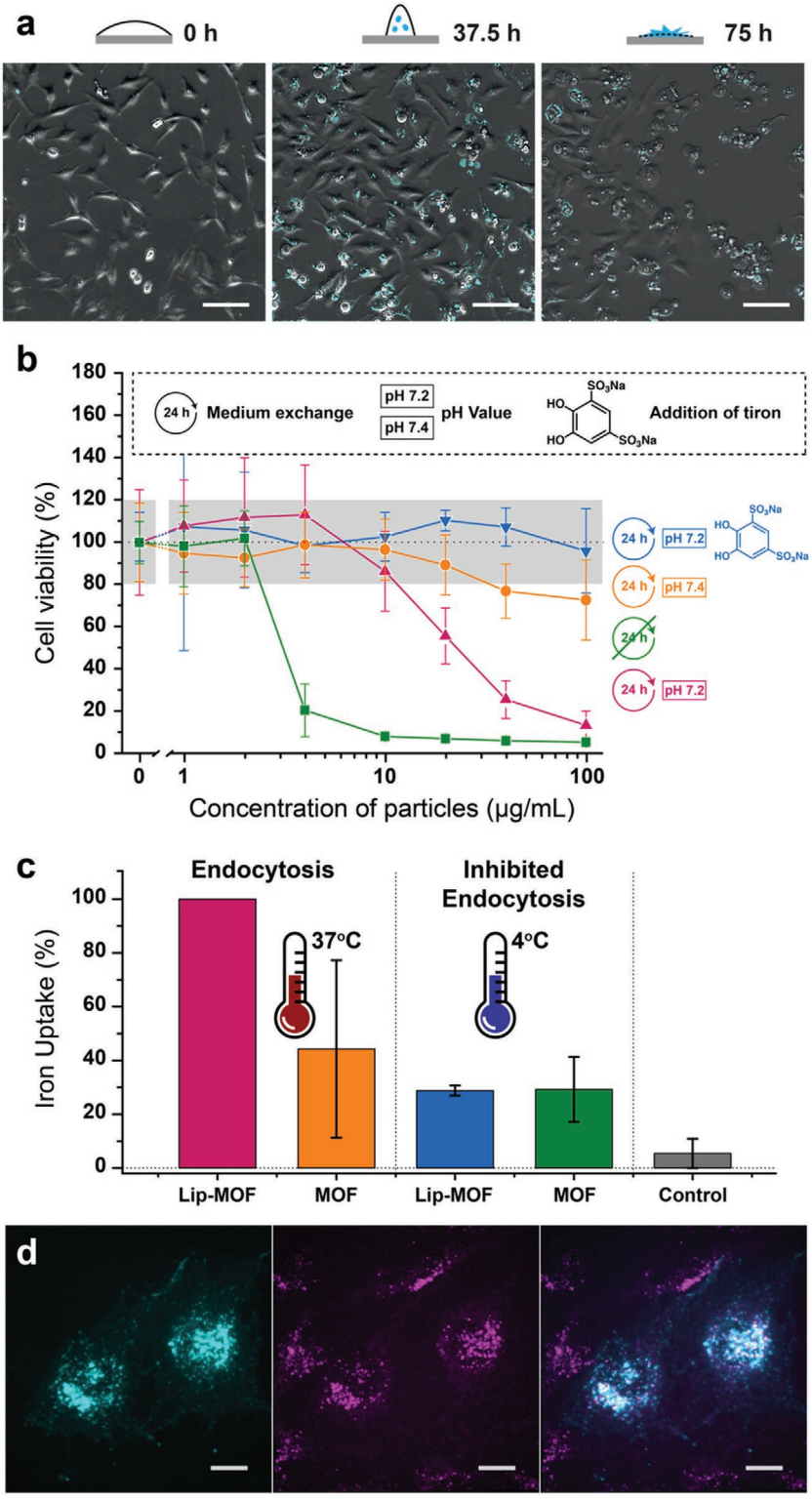

Figure 2. Uptake and cell viability of Lip-MOF in cells. a) Time-lapse images of Lip-MOF on HeLa cells. Overlay of bright-field (grayscale) and fluorescence (cyan) images at 0, 37.5, and 75 h after incubation of HeLa cells with calcein-loaded Lip-MOF. Over time, Lip-MOF degrade as visualized by the increase in calcein fluorescence (cyan). Subsequently, cell lysis is observed. A schematic representation of cell shape at the respective time points is shown on top of each image. Scale bar: 100 µm. b) Cell viability after Lip-MOF incubation for 72 h measured via a MTT assay. Incubation without medium exchange (green squares) leads to cell death. Medium exchange to pH 7.4 (orange circles) every 24 h restores cell viability. Medium exchange to pH 7.2 (red triangles) every 24 h did not prevent cell death. Addition of the iron-chelating compound Tiron (blue triangles) after 24 h restores cell viability. The mean values and standard deviations represent the average of biological triplicates. Each data set is normalized to cells growing under the same conditions but without exposure to Lip-MOF. The gray background is a guide to the eye indicating no significant toxicity. c) Iron uptake of HeLa cells measured by ICP-OES after incubation of Lip-MOF and uncoated MOF nanoparticles at 37 and 4 °C. Values are normalized to iron uptake for Lip-MOF at 37 °C. The negative control is without MOF addition. d) Confocal microscopy images of HeLa cells incubated with Atto647N-loaded Lip-MOF after 40 h incubation without medium exchange. Lysosomes (cyan) and nanoparticles (magenta) are colocalized as shown in white in the merged image on the right. Lysosomes were labeled by transiently transfecting the cells with CellLight Lysosomes-GFP. Scale bar: 25 µm.

enzymes is very unlikely due to their specificity and steric hindrances. Accordingly, none of the tested inhibitors of various lysosomal hydrolases had an effect on the toxicity of Lip-MOF (Figure S11, Supporting Information). Also, the acidic pH of the lysosome can be excluded as the reason for degradation, since addition of HCl does not degrade the MOF nanoparticles (Figure S12, Supporting Information). However, lysosomes contain a high amount of cysteines[16] and the reductive milieu created by cysteines destroys MIL-100(Fe) as shown in **Figure 3**a. The reaction kinetics displayed in Figure 3b (cf. also Figures S13 and S14, Supporting Information) exhibits a delay of the process by at least 5 min. Any enzyme-driven reaction in the lysosome relying on cysteines will be faster. Thus, the delay allows for the maintenance of reactions that rely on cysteines, such as scavenging of reactive oxygen species. Furthermore, it suggests that the reaction can only take place in the excess of cysteines. Accordingly, the amount of lysosomal cysteines and thus its reductive potential should influence the degradation of Lip-MOF in cells. Indeed, addition of 5×10^{-3} M *N*-acetyl-cysteine (Figure 3c) or GSH (Figure S15a, Supporting Information) into the medium enhanced the efficiency of Lip-MOF to induce cell death. In addition, $ZnSO_4$ reduced the effect that Lip-MOF had on cells (Figure S15b, Supporting Information), most likely due to Zn^{2+} binding to cysteines and thereby reducing the amount of active cysteines.[17] The dependence on lysosomal cysteines and their reductive potential explains the dependence of the effect on extracellular pH: the reductive

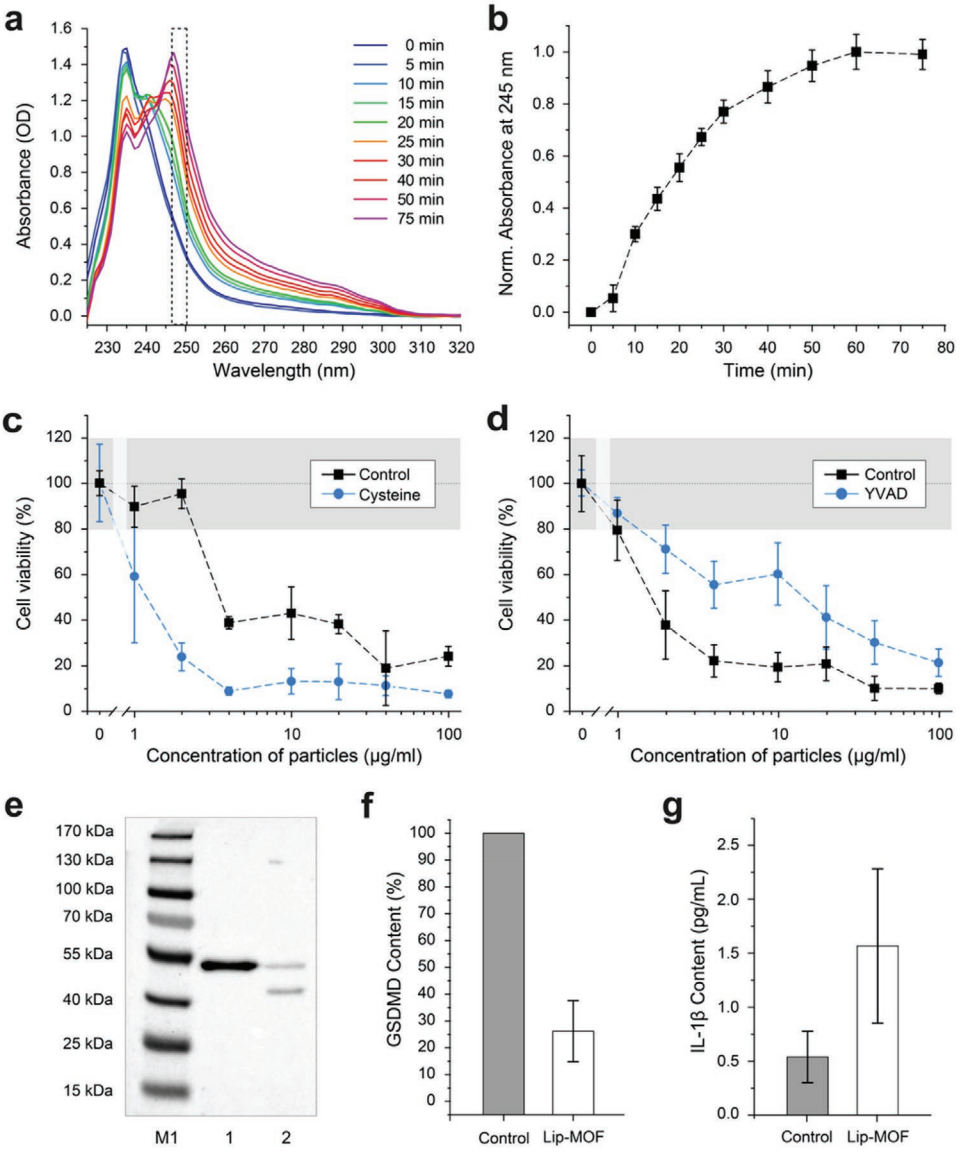

Figure 3. Chemical degradation of MOF nanoparticles and pyroptosis. a) Absorbance spectra of cysteine and trimesic acid, which is released during degradation of MOF nanoparticles by cysteines as a function of time. b) Absorbance of trimesic acid at 245 nm as a function of incubation time. c,d) MTT assay of HeLa cells incubated with Lip-MOF without medium exchange in the presence of: c) cysteine and d) caspase inhibitor z-YVAD-FMK (blue, circle). e,f) Anti-GSDMD Western blot of control cells (Lane 1) and cells incubated with Lip-MOF (Lane 2) showing a reduction to 25% of full length GSDMD (53 kDa). g) Anti-IL-1β ELISA assay of medium from HeLa cells incubated with Lip-MOF and phosphate-buffered saline as a control showing the release of interleukin-1β after Lip-MOF incubation as a sign for pyroptosis induced by Lip-MOF. The mean values and standard deviations represent the average of biological triplicates.

potential of HeLa cells as measured by MTT assays was already 14% higher after only 24 h at pH 7.2 as compared to pH 7.4. Also, the Raman signature of lysosomes and lipid vesicles in cells (Figure S16, Supporting Information) differs between the two pH values and confirms changes in the chemical composition revealing, among other things, a higher cysteine content and corresponding reductive potential at lower pH. At pH 7.2, the spectra showed more signal in the range of aliphatic C–S stretch vibrations[18] (630–790 cm, Figure S17 and Table S1, Supporting Information) most likely resulting from cysteines.

Next, we sought to investigate the origin of the cell bursting. Knowing that lysosomal degradation of Lip-MOF and the associated iron delivery is essential for this effect, we investigated how the high amount of iron ions generated by the Lip-MOF degradation leads to cell death. High amounts of lysosomal iron have been shown to induce ferroptosis.[3] However, as discussed above, cysteine and glutathione (Figure 3c; Figure S15a, Supporting Information) had the opposite effect, although they are known inhibitors of ferroptosis.[19] Liproxstatin, a very potent inhibitor of ferroptosis,[20] had no effect on Lip-MOF-induced cell death (Figure S15c, Supporting Information), suggesting that Lip-MOFs do not induce ferroptosis. Instead, z-YVAD-FMK, a selective caspase inhibitor[21] for pyroptosis-inducing caspases 1, 4, and 5, mitigates the effect, indicating pyroptosis as the cell

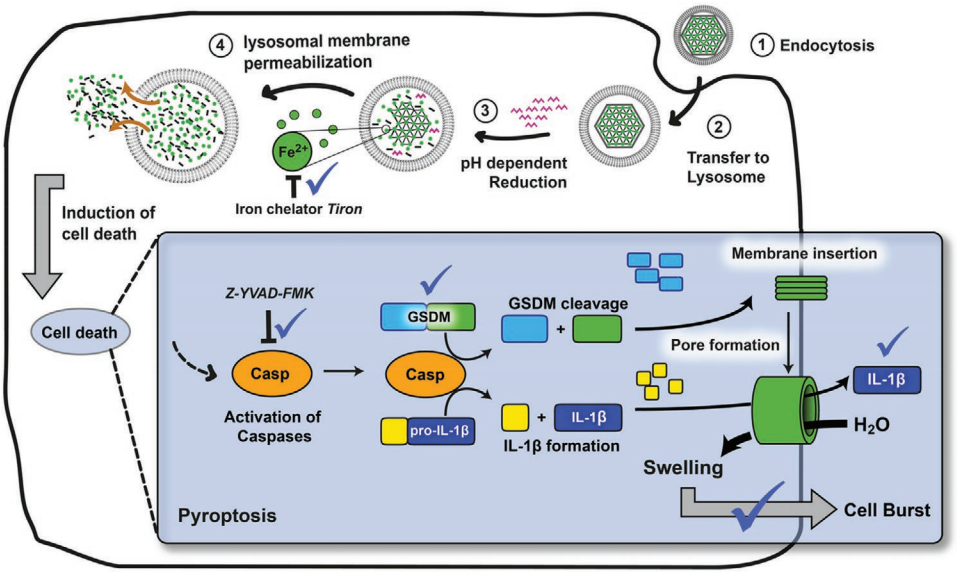

Figure 4. Uptake of Lip-MOF nanoparticles leads to pyroptosis of cells in acidic environments. The proposed uptake mechanism of MOF nanoparticles and triggered signaling pathways: 1) Uptake via clathrin-mediated endocytosis. 2) Transfer to lysosomes. 3) pH-dependent reduction and disassembly of MOFs by reducing agents like cysteines. 4) Degradation of Lip-MOF triggers lysosomal rupture and pyroptosis. Pyroptosis is mediated by caspase activation, which triggers gasdermin activation and interleukin-1β-release resulting in cell swelling and lysis.

death mechanism (Figure 3c)–especially in combination with the observed cell swelling and lysis. A similar reduction of the effect was observed in the presence of the osmolyte betaine, which has been shown to inhibit pyroptosis[22] (Figure S15d, Supporting Information). Pyroptosis is mediated by caspase-induced gasdermin cleavage followed by gasdermin pore formation in the cell membrane.[23] These gasdermin pores perforate the cell membrane inducing IL-1β release and cell swelling until they burst.[24] Indeed, we found a significant reduction of full-length gasdermin D (GSDMD) in Western blots of Lip-MOF-treated cells (Figure 3d,f; Figure S18, Supporting Information). The length of the GSDMD cleavage product suggests caspase-3 activity, which has been reported to induce pyroptosis via GSDME activation.[25] We also observe IL-1β released into the medium. Thus, Lip-MOF induces pyroptosis after degradation by cysteines in cells with a high reductive potential at slightly acidic pH. Iron has been reported to trigger pyroptosis mediated by reactive oxygen species (ROS) production.[26] However, we did not observe any ROS (Figure S19, Supporting Information), nor did the ROS inhibitors cysteine or Liproxstatin (Figure 3c; Figure S15c, Supporting Information) inhibit the effect, suggesting that ROS does not play a role in Lip-MOF-induced pyroptosis. Another possible pathway for the observed pyroptosis could be via the BCL family members BAX[27] and BCL-2.[28] But neither inhibition of BCL-2 nor activation of BAX had any impact on the efficiency of pyroptosis induction by Lip-MOF (Figure S20, Supporting Information).[29] Thus, the effect is supposedly independent of BAX and BCL-2 concentrations. To test whether the effect found for HeLa cells applies to other cell types as well, we performed experiments with several other cell lines. We found the pyroptosis-inducing effect of Lip-MOF being present also in A431 and MCF7 cells, but not in A549 cells (Figure S21a–c, Supporting Information), suggesting that A549 cells are more tolerant toward high concentrations of lysosomal iron. Non-tumorigenic breast cells MCF-10A were significantly less affected (Figure S21d, Supporting Information) than breast cancer cells MCF-7 (Figure S21a, Supporting Information). Finally, we tested the effect of Lip-MOF on macrophages. Macrophages have been reported to show activation in response to other iron formulations.[30] Moreover, they are present in tumor environments and internalize the majority of administered nanoparticles.[31] Upon incubation with Lip-MOF, macrophages clearly showed pyroptosis. The observed pyroptosis was dependent on extracellular pH similarly to HeLa cells (Figure S22, Supporting Information). Thus, a possible immune stimulus will not be hampered, if most of the administered nanoparticles are taken up by macrophages in the tumor environment rather than by tumor cells. These results encourage future studies on the underlying molecular mechanism as a basis for future successful translation in vivo.

In conclusion, we have demonstrated that the synergistic combination of lipids and MOF nanoparticles exploits the advantageous properties of each system to create a controllable platform for intracellular iron delivery. The lipid coating facilitates stealth endolysosomal uptake and the MOF nanoparticles release their building blocks into the cell. Together, they overcome cellular regulation and deliver high amounts of iron ions into the cell. This process is controlled by the extracellular pH via the intracellular reductive potential. Ultimately, pyroptosis is induced by caspase activation followed by GSDMD cleavage and cell lysis (**Figure 4**). This unprecedented property of lipid-coated MOF nanoparticles may be used in the future for investigations of the effects of ion overdoses. Based on the tunability of MOF nanoparticles, the degradation kinetics, amount of released ions, and the specific type of released ion may be varied and investigated. This controlled ion delivery to cells in spatially confined microenvironments may pave the way for further nanomaterials with applications based on this

property. As an example, Lip-MOFs and similar nanostructures may be applied in immunotherapy for attacking tumor cells in the acidic tumor environment directly via pyroptosis and at the same time eliciting an immune response.

Supporting Information

Supporting Information is available from the Wiley Online Library or from the author.

Acknowledgements

The authors thank Jana Peliskova for experimental support. Funding by the Center for NanoScience Munich (CeNS) and by the Deutsche Forschungsgemeinschaft (SFB1032, Project-ID 201269156-SFB1032, B03, B08, and B11; WU 622/4-1; PL 696/4-1) is gratefully acknowledged.

Conflict of Interest

The authors declare no conflict of interest.

Author Contributions

E.P. and A.Z. contributed equally to this work. H.E., S.W., and V.C. conceived the idea with S.Z. and A.M.V. providing additional advice. A.M.V. had the idea of pyroptosis. The project was carried out under the supervision of H.E. A.Z. prepared and characterized the MOF nanoparticles under the supervision of S.W. and H.E. A.Z. and H.E. coated the particles with lipids. H.E. carried out and designed cell experiments with a support from A.Z. and guidance from S.Z. and A.M.V. E.P., D.B., and C.H. carried out Raman experiments. E.P., A.Z., and D.B. analyzed the data. E.P. and H.E. conducted the statistical analysis. E.P. designed the figures. D.C.L. contributed additional support. E.P., A.Z., H.E., and S.W. wrote the manuscript with input from all authors.

Keywords

bionanotechnology, intracellular ion delivery, metal–organic frameworks, nanoparticles, pyroptosis

Received: November 5, 2019
Revised: March 1, 2020
Published online:

[1] a) D. E. Clapham, *Cell* **2007**, *131*, 1047; b) M. U. Muckenthaler, S. Rivella, M. W. Hentze, B. Galy, *Cell* **2017**, *168*, 344.
[2] S. Orrenius, B. Zhivotovsky, P. Nicotera, *Nat. Rev. Mol. Cell Biol.* **2003**, *4*, 552.
[3] S. J. Dixon, K. M. Lemberg, M. R. Lamprecht, R. Skouta, E. M. Zaitsev, C. E. Gleason, D. N. Patel, A. J. Bauer, A. M. Cantley, W. S. Yang, B. Morrison, B. R. Stockwell, *Cell* **2012**, *149*, 1060.
[4] M. Wessling-Resnick, *Annu. Rev. Nutr.* **2010**, *30*, 105.
[5] I. Alfonso, R. Quesada, *Chem. Sci.* **2013**, *4*, 3009.
[6] a) T. Simon-Yarza, A. Mielcarek, P. Couvreur, C. Serre, *Adv. Mater.* **2018**, *30*, 1707365; b) S. Wang, C. M. McGuirk, A. d'Aquino, J. A. Mason, C. A. Mirkin, *Adv. Mater.* **2018**, *30*, 1800202; c) R. Freund, U. Lächelt, T. Gruber, B. Rühle, S. Wuttke, *ACS Nano* **2018**, *12*, 2094; d) I. Abánades Lázaro, R. S. Forgan, *Coord. Chem. Rev.* **2019**, *380*, 230; e) J. F. Mukerabigwi, Z. Ge, K. Kataoka, *Chem. - Eur. J.* **2018**, *24*, 15706.
[7] a) H. Furukawa, K. E. Cordova, M. O'Keeffe, O. M. Yaghi, *Science* **2013**, *341*, 1230444; b) Z. Dong, Y. Sun, J. Chu, X. Zhang, H. Deng, *J. Am. Chem. Soc.* **2017**, *139*, 14209.
[8] a) S. Nagata, K. Kokado, K. Sada, *Chem. Commun.* **2015**, *51*, 8614; b) I. Abanades Lazaro, S. Haddad, S. Sacca, C. Orellana-Tavra, D. Fairen-Jimenez, R. S. Forgan, *Chem* **2017**, *2*, 561.
[9] a) S. Wang, W. Morris, Y. Liu, C. M. McGuirk, Y. Zhou, J. T. Hupp, O. K. Farha, C. A. Mirkin, *Angew. Chem.* **2015**, *127*, 14951; b) B. Illes, P. Hirschle, S. Barnert, V. Cauda, S. Wuttke, H. Engelke, *Chem. Mater.* **2017**, *29*, 8042.
[10] a) P. Horcajada, S. Surblé, C. Serre, D.-Y. Hong, Y.-K. Seo, J.-S. Chang, J.-M. Grenèche, I. Margiolaki, G. Férey, *Chem. Commun.* **2007**, 2820; b) P. Horcajada, T. Chalati, C. Serre, B. Gillet, C. Sebrie, T. Baati, J. F. Eubank, D. Heurtaux, P. Clayette, C. Kreuz, J. S. Chang, Y. K. Hwang, V. Marsaud, P. N. Bories, L. Cynober, S. Gil, G. Ferey, P. Couvreur, R. Gref, *Nat. Mater.* **2010**, *9*, 172.
[11] D. Tang, R. Kang, T. V. Berghe, P. Vandenabeele, G. Kroemer, *Cell Res.* **2019**, *29*, 347.
[12] a) A. Zimpel, T. Preiß, R. Röder, H. Engelke, M. Ingrisch, M. Peller, J. O. Rädler, E. Wagner, T. Bein, U. Lächelt, S. Wuttke, *Chem. Mater.* **2016**, *28*, 3318; b) S. Wuttke, S. Braig, T. Preiß, A. Zimpel, J. Sicklinger, C. Bellomo, J. O. Rädler, A. M. Vollmar, T. Bein, *Chem. Commun.* **2015**, *51*, 15752; c) S. Wuttke, A. Zimpel, T. Bein, S. Braig, K. Stoiber, A. Vollmar, D. Müller, K. Haastert-Talini, J. Schaeske, M. Stiesch, G. Zahn, A. Mohmeyer, P. Behrens, O. Eickelberg, D. A. Bölükbas, S. Meiners, *Adv. Healthcare Mater.* **2017**, *6*, 1600818.
[13] a) J. Liu, X. Jiang, C. Ashley, C. J. Brinker, *J. Am. Chem. Soc.* **2009**, *131*, 7567; b) B. Illes, S. Wuttke, H. Engelke, *Nanomaterials* **2017**, *7*, 351.
[14] P. W. Hochachka, T. P. Mommsen, *Science* **1983**, *219*, 1391.
[15] a) C. Orellana-Tavra, S. A. Mercado, D. Fairen-Jimenez, *Adv. Healthcare Mater.* **2016**, *5*, 2261; b) R. Röder, T. Preiß, P. Hirschle, B. Steinborn, A. Zimpel, M. Höhn, J. O. Rädler, T. Bein, E. Wagner, S. Wuttke, U. Lächelt, *J. Am. Chem. Soc.* **2017**, *139*, 2359.
[16] J. B. Lloyd, *Biochem. J.* **1986**, *237*, 271.
[17] N. J. Pace, E. Weerapana, *Biomolecules* **2014**, *4*, 419.
[18] G. Socrates, *Infrared and Raman Characteristic Group Frequencies: Tables and Charts*, Wiley, Chichester, UK **2004**.
[19] S. E. Kim, L. Zhang, K. Ma, M. Riegman, F. Chen, I. Ingold, M. Conrad, M. Z. Turker, M. Gao, X. Jiang, S. Monette, M. Pauliah, M. Gonen, P. Zanzonico, T. Quinn, U. Wiesner, M. S. Bradbury, M. Overholtzer, *Nat. Nanotechnol.* **2016**, *11*, 977.
[20] a) O. Zilka, R. Shah, B. Li, J. P. Friedmann Angeli, M. Griesser, M. Conrad, D. A. Pratt, *ACS Cent. Sci.* **2017**, *3*, 232; b) J. P. Friedmann Angeli, M. Schneider, B. Proneth, Y. Y. Tyurina, V. A. Tyurin, V. J. Hammond, N. Herbach, M. Aichler, A. Walch, E. Eggenhofer, D. Basavarajappa, O. Radmark, S. Kobayashi, T. Seibt, H. Beck, F. Neff, I. Esposito, R. Wanke, H. Forster, O. Yefremova, M. Heinrichmeyer, G. W. Bornkamm, E. K. Geissler, S. B. Thomas, B. R. Stockwell, V. B. O'Donnell, V. E. Kagan, J. A. Schick, M. Conrad, *Nat. Cell Biol.* **2014**, *16*, 1180.
[21] E. Yakut, C. Jakobs, A. Peric, G. Michel, N. Baal, G. Bein, B. Brune, V. Hornung, H. Hackstein, *J. Immunol.* **2015**, *194*, 2569.
[22] Y. Xia, S. Chen, G. Zhu, R. Huang, Y. Yin, W. Ren, *Front. Immunol.* **2018**, *9*, 2670.
[23] a) J. Shi, W. Gao, F. Shao, *Trends Biochem. Sci.* **2017**, *42*, 245; b) L. Galluzzi, I. Vitale, S. A. Aaronson, J. M. Abrams, D. Adam, P. Agostinis, E. S. Alnemri, L. Altucci, I. Amelio, D. W. Andrews, M. Annicchiarico-Petruzzelli, A. V. Antonov, E. Arama, E. H. Baehrecke, N. A. Barlev, N. G. Bazan, F. Bernassola, M. J. M. Bertrand, K. Bianchi, M. V. Blagosklonny, K. Blomgren, C. Borner, P. Boya, C. Brenner, M. Campanella, E. Candi,

D. Carmona-Gutierrez, F. Cecconi, F. K. M. Chan, N. S. Chandel, *Cell Death Differ.* **2018**, *25*, 486.

[24] K. Nagarajan, K. Soundarapandian, R. F. Thorne, D. Li, D. Li, *Transl. Oncol.* **2019**, *12*, 925.

[25] Y. Wang, W. Gao, X. Shi, J. Ding, W. Liu, H. He, K. Wang, F. Shao, *Nature* **2017**, *547*, 99.

[26] K. Nakamura, T. Fujiwara, T. Ishii, H. Harigae, K. Ogasawara, *Blood* **2014**, *124*, 2723.

[27] J. E. Vince, D. De Nardo, W. Gao, A. J. Vince, C. Hall, K. McArthur, D. Simpson, S. Vijayaraj, L. M. Lindqvist, P. Bouillet, M. A. Rizzacasa, S. M. Man, J. Silke, S. L. Masters, G. Lessene, D. C. S. Huang, D. H. D. Gray, B. T. Kile, F. Shao, K. E. Lawlor, *Cell Rep.* **2018**, *25*, 2339.

[28] C.-S. Shi, J. H. Kehrl, *Cell Death Discovery* **2019**, *5*, 151.

[29] a) A. J. Souers, J. D. Leverson, E. R. Boghaert, S. L. Ackler, N. D. Catron, J. Chen, B. D. Dayton, H. Ding, S. H. Enschede, W. J. Fairbrother, D. C. S. Huang, S. G. Hymowitz, S. Jin, S. L. Khaw, P. J. Kovar, L. T. Lam, J. Lee, H. L. Maecker, K. C. Marsh, K. D. Mason, M. J. Mitten, P. M. Nimmer, A. Oleksijew, C. H. Park, C.-M. Park, D. C. Phillips, A. W. Roberts, D. Sampath, J. F. Seymour, M. L. Smith, G. M. Sullivan, S. K. Tahir, C. Tse, M. D. Wendt, Y. Xiao, J. C. Xue, H. Zhang, R. A. Humerickhouse, S. H. Rosenberg, S. W. Elmore, *Nat. Med.* **2013**, *19*, 202; b) E. Gavathiotis, D. E. Reyna, J. A. Bellairs, E. S. Leshchiner, L. D. Walensky, *Nat. Chem. Biol.* **2012**, *8*, 639.

[30] S. Zanganeh, G. Hutter, R. Spitler, O. Lenkov, M. Mahmoudi, A. Shaw, J. S. Pajarinen, H. Nejadnik, S. Goodman, M. Moseley, L. M. Coussens, H. E. Daldrup-Link, *Nat. Nanotechnol.* **2016**, *11*, 986.

[31] a) M. A. Miller, S. Gadde, C. Pfirschke, C. Engblom, M. M. Sprachman, R. H. Kohler, K. S. Yang, A. M. Laughney, G. Wojtkiewicz, N. Kamaly, S. Bhonagiri, M. J. Pittet, O. C. Farokhzad, R. Weissleder, *Sci. Transl. Med.* **2015**, *7*, 314ra183; b) Q. Dai, S. Wilhelm, D. Ding, A. M. Syed, S. Sindhwani, Y. Zhang, Y. Y. Chen, P. MacMillan, W. C. W. Chan, *ACS Nano* **2018**, *12*, 8423.